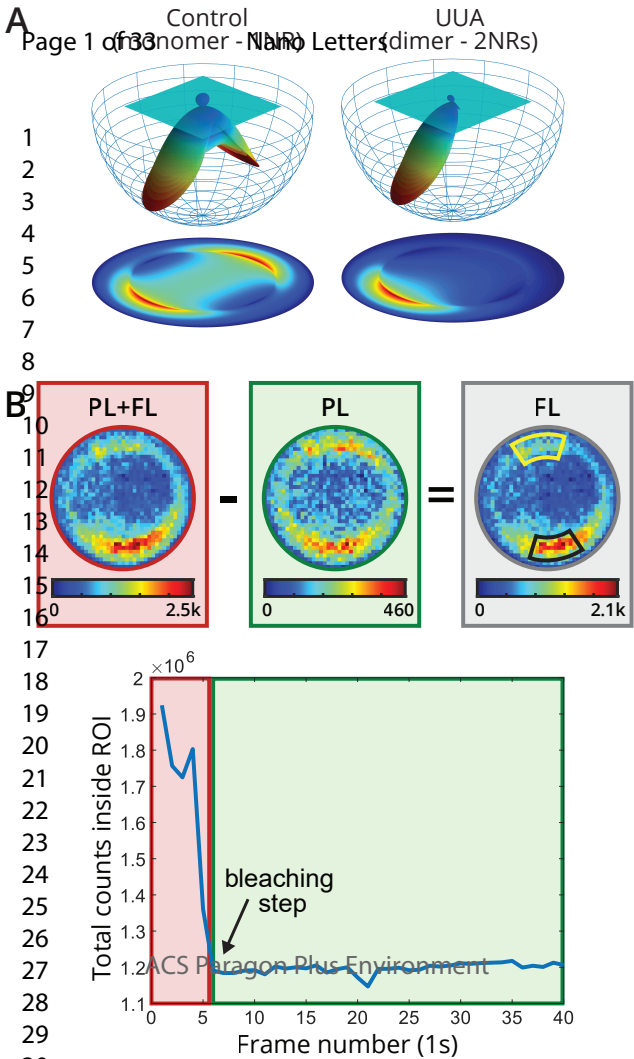

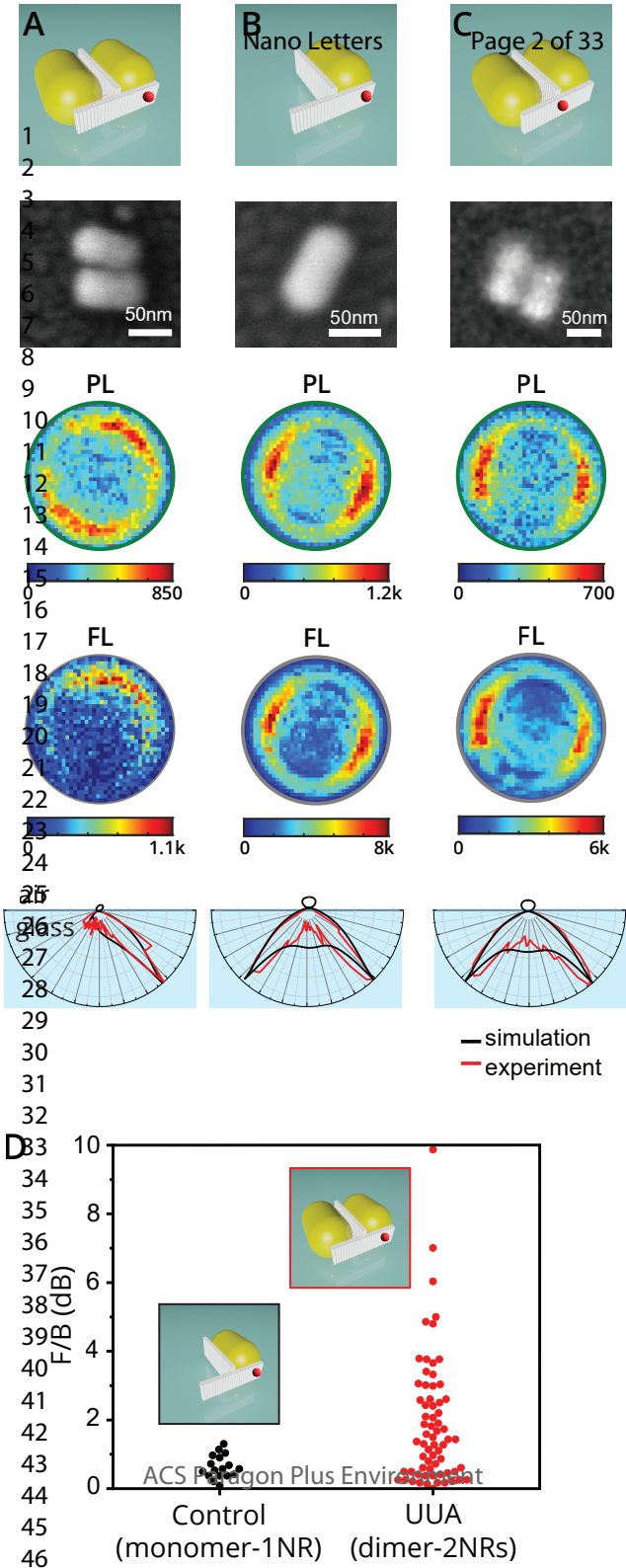

DNA-templated ultracompact optical antennas for unidirectional single-molecule emission

Fangjia Zhu[1]‡, María Sanz-Paz[1]‡, Antonio I. Fernández-Domínguez[2], Xiaolu Zhuo[3,4], Luis M. Liz-Marzán[3,4,5], Fernando D. Stefani[6,7], Mauricio Pilo-Pais[1]*, and Guillermo P. Acuna[1]*.*

[1]Department of Physics, University of Fribourg; Fribourg CH-1700, Switzerland.

[2]Departamento de Física Teórica de la Materia Condensada and Condensed Matter Physics Center (IFIMAC), Universidad Autónoma de Madrid; E-28049 Madrid, Spain.

[3]CIC biomaGUNE, Basque Research and Technology Alliance (BRTA); Donostia-San Sebastian 20014, Spain.

[4]Centro de Investigación Biomédica en Red de Bioingeniería, Biomateriales y Nanomedicina (CIBER-BBN); Donostia-San Sebastian 20014, Spain.

[5]Ikerbasque, Basque Foundation for Science; 48009 Bilbao, Spain.

[6]Centro de Investigaciones en Bionanociencias (CIBION), Consejo Nacional de Investigaciones Científicas y Técnicas (CONICET); C1425FQD Ciudad Autónoma de Buenos Aires, Argentina.

[7]Departamento de Física, Facultad de Ciencias Exactas y Naturales, Universidad de Buenos Aires; C1428EHA Ciudad Autónoma de Buenos Aires, Argentina.

KEYWORDS nanophotonics, optical antennas, plasmonics, single-molecule fluorescence, single-photon sources, colloidal nanoparticles, DNA nanotechnology, DNA origami.

ABSTRACT

Optical antennas are nanostructures designed to manipulate light-matter interactions by interfacing propagating light with localized optical fields. In recent years, a plethora of devices have been realized to efficiently tailor the absorption and/or emission rates of fluorophores. By contrast, modifying the spatial characteristics of their radiation fields remains challenging. Successful phased array nanoantenna designs have required the organization of several elements over a footprint comparable to the operating wavelength. Here, we report unidirectional emission of a single fluorophore using an ultracompact optical antenna. The design consists of two side-by-side gold nanorods self-assembled via DNA origami, which also controls the positioning of the single-fluorophore. Our results show that when a single fluorescent molecule is positioned at the tip of

one nanorod and emits at a frequency capable of driving the antenna in the anti-phase mode, unidirectional emission with a forward to backward ratio of up to 9.9 dB can be achieved.

Light-matter interactions at the nanoscale are limited by the two orders of magnitude size mismatch between the electronic confinement of quantum emitters (in the Å to nm range) and the wavelength of the optical radiation (in the hundreds of nm range). In analogy to their microwave or radiofrequency counterparts, optical antennas can act as transducers between propagating light and localized fields. To date, a plentiful library of optical antennas has been designed and demonstrated[1,2], improving by several orders of magnitude the rates of light absorption and emission of individual photon emitters[3]. Specifically, plasmon-induced localized fields have been extensively exploited to enhance single-molecule spectroscopic signals including fluorescence[4] and Raman scattering[5]. A less studied aspect of optical antennas is their ability to impose directionality of the emitted light[6].

Photon absorption and emission involve dipolar, or under special conditions multipolar[7], transition moments, and therefore do not possess intrinsic unidirectionality. Thus, artificial

schemes to increase the directionality of photon emitters are of crucial significance, for example in the context of integrated optical circuits and quantum communication/computing schemes[8,9].

Over a decade ago, Curto *et al.* used lithographically-made Yagi-Uda antennas to demonstrate the unidirectional emission of quantum dots[10]. A drawback of such phased array antennas is that they require placing various elements at distances of around λ/4[11,12], which extends their footprint to dimensions larger than the wavelength. Several more compact directional designs aiming to reduce the overall effective size by an order of magnitude have been proposed and numerically investigated[13]. One strategy for ultracompact unidirectional antennas exploits the interplay of spectrally overlapping electric and magnetic resonances of single high-index dielectric nanoparticles[14], or arrangements of metallic nanoparticles that can support both electric and magnetic modes in the same spectral range[15]. Alternatively, Pakizeh *et al.*[16] proposed a design of two gold nanodisks separated by 10 nm. A photon emitter in the vicinity of one of the disks drives the resonance of the two metallic disks with a phase delay between each other introduced by the separation gap, resulting in unidirectional emission at frequencies close to the anti-phase plasmon mode of the system[16].

Even though the potential and working principles of undirectional ultracompact antennas for single emitters have been long known, their experimental realization remained elusive due to several shortcomings of traditional top-down nanofabrication methods. For instance, top-down methods can hardly produce the reduced gaps under 20 nm necessary for ultracompact antennas, and more importantly, they do not allow placing single emitters near an optical antenna element with positional and stoichiometric control.

In this work, we report the realization of an ultracompact directional antenna for single-photon emitters produced by means of DNA self-assembly. The DNA origami technique[17-19] was used to assemble two colloidal gold nanorods (AuNRs) in a side-to-side arrangement with a controlled separation gap, and a single fluorescent molecule at the tip of one of the AuNRs.

Results

The geometry and working principle of the ultracompact unidirectional antenna (UUA) driven in anti-phase is schematically shown in Figure 1A. Two identical AuNRs are placed side by side, and a single dipolar emitter (black arrow) is placed at the tip of one of the AuNRs. The overall emission can be approximated by the sum of the induced dipolar oscillations in each element (blue

and red arrows). Depending on the geometry, materials, and wavelength (frequency of the emitter), conditions can be met where constructive and destructive interference occur at opposite sides of the UUA, leading to unidirectional emission. To illustrate this, Figure 1B shows schematically the calculated angular emission pattern of a UUA driven in anti-phase, along with the emission pattern of a single AuNR (monomer antenna).

To fabricate these UUAs, we used a T-shaped DNA origami host structure (Figure 1C) as a template to assemble through DNA hybridization previously functionalized colloidal AuNRs in a side-to-side configuration (Figure 1D) with a separation gap of 5 nm (further details are included in Figure S1 and Table S1). The origami design enables the incorporation of a single fluorescent molecule at the tip of one of the AuNRs, 5 nm away from the gold surface (red dot in Figures 1C and D). AuNRs with nominal dimensions of 40 nm in diameter and 68 nm in length were self-assembled in solution with the DNA origami to form the UUAs, which were then purified by gel electrophoresis and imaged by transmission electron microscopy (TEM), confirming the correct self-assembly of our structures (Figure 1E). Some degree of variability in the dimensions of the AuNRs is observed, in agreement with the size distribution of the colloid. Considering these

dimensions, UUAs have an overall size of 85×73 nm^2, an order of magnitude smaller than phased-array (Yagi-Uda) configurations[11,12].

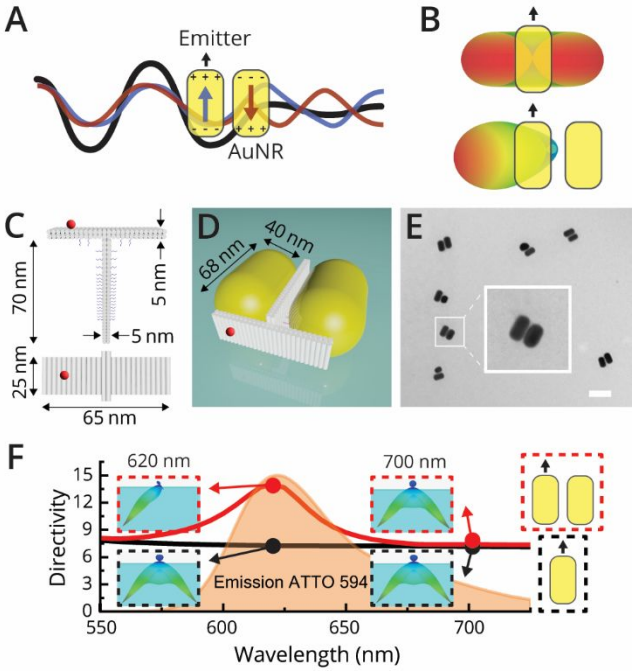

Figure 1. Geometry and working principle of a unidirectional ultracompact antenna (UUA) based on two gold nanorods (AuNRs) placed side-to-side. (A) If the quadrupole-like anti-phase mode is excited by a dipolar source (black arrow) in the near-field of one element, constructive and destructive interferences can be achieved at opposite sides of the antenna, leading to unidirectional emission. Red and blue solid lines represent the emission from each rod whereas the black solid line represents their sum. (B) Calculated angular emission patterns for a single AuNR (monomer

antenna) and a UUA (dimer) driven by a single dipolar source in vacuum. (C, D) Sketch of the DNA origami host structure (C) and the assembled antenna (D) with a single photon emitter (red dot). (E) TEM image of UUAs, scale bar 200 nm. (F) Spectral directivity for both a UUA with the geometry described in (C), and a monomer antenna placed on a glass substrate, together with the emission spectra of ATTO 594. The insets show the emission pattern close to the anti-phase mode wavelength (620 nm) and away from it (700 nm).

The expected spectral response of the UUAs on a glass substrate was investigated numerically by means of finite element simulations. The directivity vs. wavelength and exemplary emission patterns of a UUA (red line) and a monomer antenna (black line) are shown in Figure 1F. Strong unidirectional emission is predicted for emitters with an emission wavelength from 600 to 630 nm, where the UUA is driven in anti-phase[20]. These wavelengths are red-shifted from both the longitudinal resonance of a single AuNR and the in-phase resonance of the UUA (see Figure S2). Thus, a fluorophore emitting in this range (e.g., ATTO 594, Figure 1F), is expected to show unidirectional emission when coupled to the UUA, detectable for instance by the very distinct

back-focal plane (BFP) images[21] when compared to the dipolar emission from the monomer antenna control (Figure 2A).

The performance of the fabricated UUAs was studied experimentally in a custom-built scanning fluorescence microscope modified to relay the BFP image of the structure into a CCD (see details in Methods). For each UUA, a series of BFP images was acquired, from which an intensity transient was generated (Figure 2B). Only transients with a single bleaching step, a signature of emission arising from a single fluorophore, were employed for further analysis. This approach, in addition to confirming that only one molecule was driving the antenna, enabled the discrimination of the single-molecule fluorescence (FL) emission from photoluminescence (PL) of AuNRs[22]. This analysis was combined with scanning electron microscopy (SEM) imaging to correlate the antenna structure with the directionality of single-molecule emission.

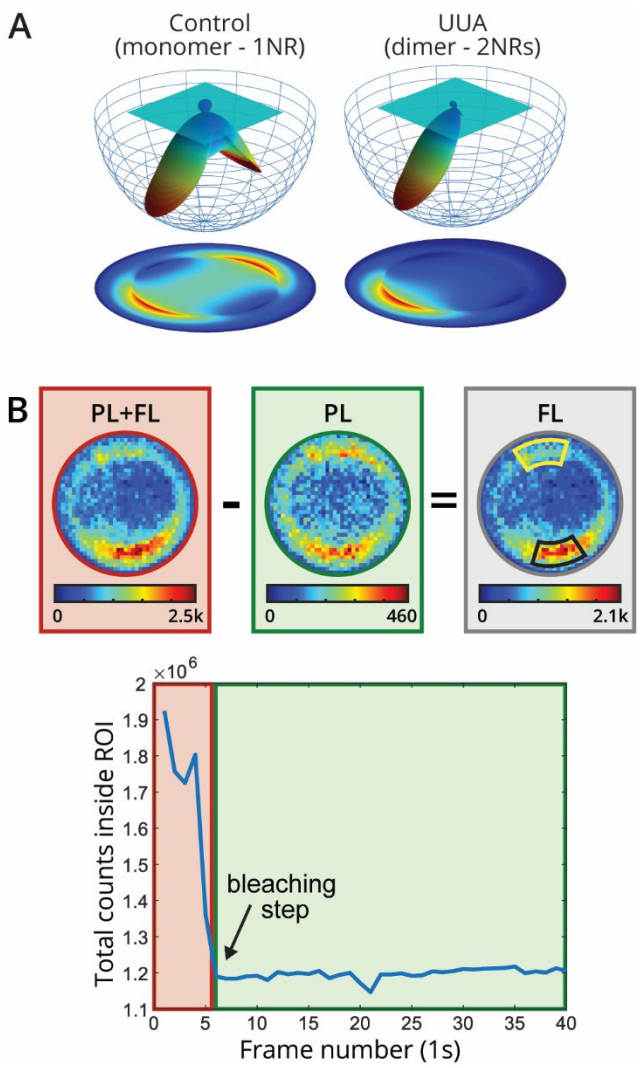

Figure 2. Back-focal plane imaging and analysis pipeline. (A) Simulated back-focal plane images for the monomer antenna and the UUA. (B) Determination of fluorescence (FL) and photoluminescence (PL) patterns from back-focal plane (BFP) imaging. For each antenna, a series of BFP images were acquired. From the integrated intensity transient, the time point where the single ATTO 594 fluorophore bleaches is identified. The BFP image corresponding to FL emission by the single fluorophore is obtained by subtracting the averaged BFP image before (PL+FL) and

after (PL) bleaching. From this pattern, we integrate the pixels in a sector containing the highest signal (black sector) and divide by the opposite sector (yellow) to obtain the forward-to-backward ratio (F/B).

An exemplary result for a UUA is shown in Figure 3A. The PL BFP image shows a symmetric pattern with two lobes of similar intensity, separated by a line of minimum intensity parallel to the AuNRs, as determined from the SEM image. This emission pattern is characteristic of a dipolar emitter and can be rationalized based on the symmetry of the structure and the fact that PL emission corresponds to far-field excitation of the in-phase plasmon dipolar mode. The situation changes for the FL emission when the UUA is driven in anti-phase by the single fluorophore in the near-field. The FL BFP image shows a single lobe of high intensity indicating unidirectional emission. More examples of UUAs are shown in Figure S3.

The directionality achieved with this ultracompact design depends critically not only on the positioning of the antenna elements but also on the position of the emitter. To demonstrate this, we exploited the unique flexibility and nanometer positioning control of the DNA origami technique to self-assemble a monomer antenna (Figure 3B) and a symmetric dimer antenna where

the single ATTO 594 fluorophore is laterally shifted to a position equidistant to the two AuNRs (Figure 3C). In these two cases, both BFP images of PL and FL are symmetric with two main lobes as expected for a dipolar emitter. The experimentally determined angular emission patterns for the three antenna designs are in excellent agreement with the calculations (lower panels of Figures 3A-C).

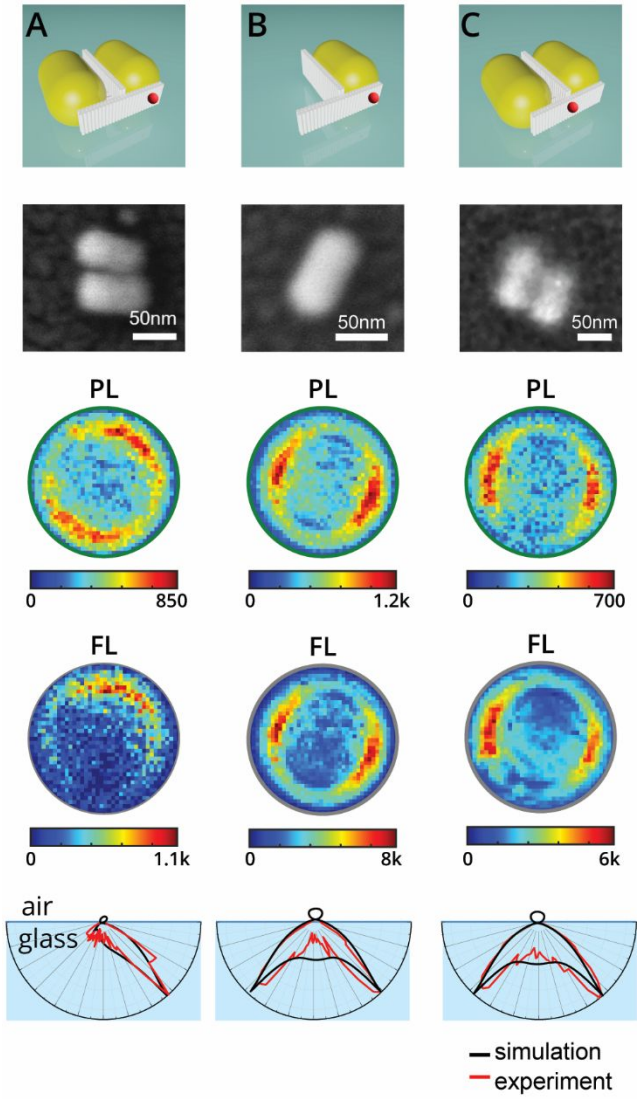
A
B
C
50nm
50nm
50nm
PL
PL
PL
0
850
0
1.2k
0
700
FL
FL
FL
0
1.1k
0
8k
0
6k
air
glass
simulation
experiment

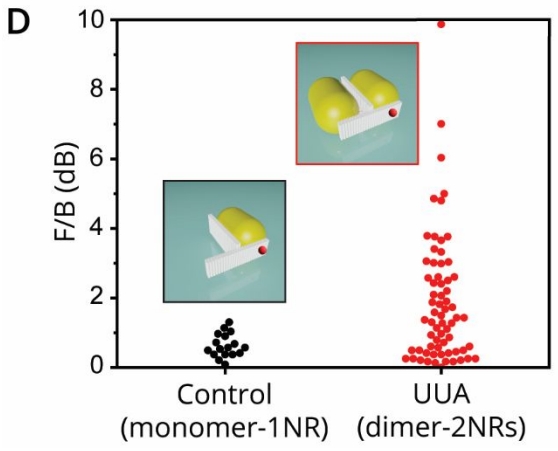
D
10
8
6
4
2
0
F/B (dB)
Control
(monomer-1NR)
UUA
(dimer-2NRs)

Figure 3. Antennas' performance. (A-C) Performance examples of a unidirectional ultracompact antenna (UUA) (A), a monomer antenna (B), and a dimer antenna with the fluorophore in the center (C). From top to bottom, 3D sketch of the structure, SEM image, BFP PL and FL images, and emission polar patterns. The position of the single fluorophore is indicated by a red dot. (D) Bee swarm distribution plots of the forward-to-backward (F/B) ratios obtained from the BFP patterns of both a monomer and a UUA. Color scale in BFP images represents counts in the camera.

Another advantage of nanofabrication based on DNA self-assembly is that it enables the parallel production of zillions of nominally identical structures. We characterized 67 UUAs and 17 monomer antennas, and quantified their performance in terms of the forward-to-backward ratio (F/B) from the BFP images using the so-called areal method[23,24] (see further details on Methods and highlighted sectors in Figure 2B). Figure 3D shows the fluorescence F/B distributions in dB for the control monomers and UUAs. While the monomer antennas should have F/B = 0 dB, experimental values range between 0 and 1.3 dB. We ascribe this residual asymmetric emission to the limited signal-to-noise ratio and slightly irregular geometry of AuNRs. In contrast, the UUAs

present a much broader distribution of F/B values, spanning a range from 0 to almost 10 dB. The maximum directionally obtained, 9.9 dB, is higher than the best reported values for top-down lithographic Yagi-Uda antennas, either driven by a single quantum dot (6 dB)[10] or electrically (9.1 dB)[23]. Several factors account for the observed distribution of F/B[25]. In addition to the signal-to-noise ratio and AuNR imperfections mentioned above for the monomer antennas, the magnitude of the directivity, as well as the spectral operating range of the UUAs, is also be affected by the size distribution of the colloidal AuNRs and their alignment in the DNA origami template (more in Figure S4).

Conclusions

We have experimentally demonstrated that the emission of a single-photon source can be mediated with a high degree of unidirectionality using an ultracompact optical antenna based on two metallic nanorods in a side-to-side configuration with deep subwavelength separation gaps of ~λ/50. This approach, theoretically predicted over a decade ago, is not based on a phased array or the interplay between magnetic and electric resonances. Instead, it uses the near-field excitation of the anti-phase mode by a dipolar emitter precisely located on top of one of the antenna elements.

This type of antenna shows a critical spectral dependency of the directionality on the geometry of the antenna. Our results confirm the theoretical predictions and show that ultracompact unidirectional optical antennas can be realized when the nanofabrication is sufficiently fine controlled, in terms of antenna elements geometry and position of the photon emitter. We addressed these challenges by bottom-up self-assembly using a T-shaped DNA origami structure to host two colloidally prepared AuNRs and a single organic fluorophore. While unidirectionality was obtained when the fluorophore was placed on top of one of the two AuNRs, it was lost when the fluorophore was shifted sideways just 22.5 nm to a position equidistant to the two AuNRs, or if only one AuNR was present. Furthermore, we achieved a maximum unidirectionality of almost 10 dB, outperforming previously reported top-down lithographic Yagi-Uda antennas based on five elements and with a footprint an order of magnitude larger.

We foresee that this work, in combination with recent advances and current efforts in DNA self-assembly[26,27], will open new routes for the fabrication of more complex nanophotonic devices, optical circuits, and light-emitting metasurfaces[28] at large scales[29,30].

Experimental Methods

Numerical simulations

Three-dimensional full-wave simulations were carried out using frequency domain solver of CST Studio Suite.

AuNRs were modeled as cylinders (R=20 nm, L=52 nm) with two semi-ellipsoidal caps (a=b=R, c=8 nm), making the total length 68 nm. For the dielectric function of gold, we used fitting data from Johnson & Christy. AuNRs were uniformly coated with 2 nm DNA layer (n_{ss}DNA = 1.7), and the gap between them was set as 5 nm. The distance between substrate and coating layer was set as 5 nm. The surrounding medium was set to air ($\varepsilon = 1$).

The scattering spectra of AuNRs on a glass substrate ($\varepsilon = 2.25$) were obtained by subtracting the scattered fields in the absence and in presence of the AuNRs. Plane waves with TE and TM polarization were used as excitation sources at normal incidence. The final simulated scattering spectra was then obtained by averaging according to $C_{sca} = \frac{1}{2}(C_{sca}^{TE} + C_{sca}^{TM})$.

For the far field pattern, a Hertzian dipole (oriented along the long axis of AuNR) was simulated as one electric dipole emitter. This dipole was placed 3 nm away from the DNA coating layer of AuNR and oriented along the AuNR´s long axis. Other orthogonal orientations had a negligible contribution to the overall signal due to quenching[25] (see Figure S5) The directivity of an antenna

is defined as $Dir_{max} = \frac{4\pi S_{max}(\theta,\ \varphi)}{\int_0^{2\pi}\int_0^{\pi} S(\theta,\ \varphi) sin\theta d\theta d\varphi}$, where $S(\theta,\varphi)$ represents the power radiated by the antenna in a given direction (θ,φ) per unit solid angle. In order to facilitate comparison with experimental BFP images, far-field radiation into the lower half-space was projected into the Fourier plane to get 2D patterns.

Forward to Backward ratio quantification

Forward to Backward ratio (F/B), defined as the integral ratio of radiated power $S(\theta,\varphi)$ in two angular ranges (($\theta_1 - \delta_1 \rightarrow \theta_1 + \delta_1$, $\varphi_1 - \delta_2 \rightarrow \varphi_1 + \delta_2$) and ($\theta_2 - \delta_1 \rightarrow \theta_2 + \delta_1$, $\varphi_2 - \delta_2 \rightarrow \varphi_2 + \delta_2$)) is used to quantify unidirectionality of antenna:

$$F/B = 10log_{10}\frac{\int_{\theta_1-\delta_1}^{\theta_1+\delta_1}\int_{\varphi_1-\delta_2}^{\varphi_1+\delta_2} S(\theta,\ \varphi) sin\theta d\theta d\varphi}{\int_{\theta_2-\delta_1}^{\theta_2+\delta_1}\int_{\varphi_2-\delta_2}^{\varphi_2+\delta_2} S(\theta,\ \varphi) sin\theta d\theta d\varphi} \quad \text{(dB)}$$

Here, (θ_1, φ_1) corresponds to the angular position of the region of maximum signal (forward direction) whereas (θ_2, φ_2) is the position of the opposite sector (backward direction), with $\theta_2 = \theta_1$ and $\varphi_2 = \varphi_1 + \pi$. Given the signal distribution in the observed BFP patterns, we chose $2\delta_1$ to cover a 6 super-pixels distance, δ_2 = 25˚ (total angular range of 50˚). Given the F/B ratio in the simulated BFP patterns, we chose δ_1=10˚.

Single molecule measurements

A sample-scanning confocal microscope with a high NA objective (Olympus, 100× NA=1.4) was modified to include a flip mirror in the detection path to switch between confocal and BFP imaging. Briefly, the BFP imaging path consists of a relay lens (f=100 mm) and a Bertrand lens (f=50 mm)[31], that produce a BFP image onto a CCD sensor (Andor iXon Ultra 888). The confocal detection is done with a single-photon counting avalanche photodiode (τ-SPAD, PicoQuant)

Measurements started with a confocal image of a region of interest in the sample from which the location of the target structures is determined. Then, the detection is switched to BFP imaging and the sample is moved to position a single structure in the center of the excitation focus. The CCD was used in kinetic mode in order to acquire videos. An integration time of 1s per frame was applied, and a sufficient number of frames was recorded (~60 frames) to allow for the observation of the bleaching step and to record PL BFP images after that. A 4×4 binning was applied during acquisition to have a higher signal per pixel[21]. This results in an emission pattern consisting of 36×36 super-pixels (1.9×1.9 mm). To achieve a good SNR, the EM gain of the camera was set to 75.

For analysis of the BFP videos, the total signal inside a circular ROI containing the pattern is retrieved and plotted as a function of the frame number. This yields an intensity time trace (see Fig. 2A) that can be used to identify the bleaching frame. Frames are averaged before (PL+FL) and after (PL) this bleaching step, and the subtraction of these two averaged images yields the average single-molecule signal (FL).

DNA origami design and folding

The T-shape DNA origami was designed using CaDNAno[32] and visualized for twist correction using CanDo[33]. Fig. S1 shows a cartoon of the origami indicating its dimensions and the positions of the modified staples. In short, the DNA template has 18x Poly-A8 (blue) and 2x Poly-A12 (green) ssDNA strands (Biomers.net GmbH) at each side that serve as handles to accommodate nanoparticles surface functionalized with Poly-T. An ATTO 594 fluorophore (red, Biomers.net GmbH) is positioned directly on top of one of the NRs, or at the top-center, as shown on Fig. S1. The design files are uploaded at https://nanobase.org/[34].

Unmodified DNA sequences were purchased from Integrated DNA Technologies INC. In short, a scaffold consisting of a vector derived from the single-stranded M13-bacteriophage genome

(M13mp18, 7249 bases, Bayou Biolabs) and staples (100 nM, ca. 32 nts) were mixed in a 1x TAE buffer (40 mM Tris, 10 mM Acetate, 1 mM EDTA, pH 8, stock purchased from Alfa, CAS#77-86-1, J63931.k3) containing 12 mM $MgCl_2$ (stock purchased from Alfa, CAS#7786-30-3, J61014.AK). The solution was heated to 75˚C and ramped down to 25˚C at a rate of 1 degree every 20 mins. The folded DNA origami structures were purified from excess staple strands by gel electrophoresis using a 0.8 % agarose gel (LE Agarose, Biozym Scientific GmbH) in a 1x TAE buffer/12 mM $MgCl_2$ buffer for 2.5 hours at 4 V/cm. The appropriate band containing the targeted DNA template was cut out and squeezed using cover slips wrapped in parafilm.

Nanorods functionalization and attachment to DNA template

Experiments were performed with AuNRs prepared following previously established protocols[35] and with commercial nanorods with nominal dimensions of 40 nm diameter and 68 nm length (Nanopartz INC.). Functionalization of both custom built and commercial AuNRs was performed in the same way. Thiolated DNA (Thiol-C6-T18, ELLA Biotech GmbH) was mixed with Au nanorods at a 100 nmol:100 uL_100 OD ratio and frozen overnight[36]. Excess DNA was removed using gel electrophoresis. This step also ensures the removal of any self-aggregated dimer formed

during the NP functionalization. The concentration of AuNRs was determined via UV-Vis absorption spectroscopy (Nanodrop).

The purified DNA template was mixed with the purified AuNRs using an excess of five AuNRs per binding site and adding NaCl to a final concentration of 600 mM. The sample was then annealed at 30˚ C and cooled down to 25˚ C at a rate of 1 degree every 30 min. This cycle was repeated 6 times. The excess of NPs was then removed by gel electrophoresis (running for 4.5 hours) and the band containing correctly formed dimers was extracted as described before.

Sample preparation

For immobilization of the structures, glass cover slips were first rinsed with water and then cleaned in a UV cleaning system (PSD Pro System, Novascan Technologies, USA). The surfaces were functionalized by sequentially immersing the substrates in the following solutions: BSA-biotin/PBS (0.5 mg/mL, Sigma Aldrich, CAS#9048-46-8, A8549-10MG) for 20 mins, neutrAvidin/PBS (0.5 mg/mL, Thermofischer, 10443985) for 20 min, and 5' biotin-Poly-A15-3' ssDNA for 20 mins (Biomers.net GmbH). In between all the steps, the coverslips were washed with 1x PBS buffer (Alfa, J75889.K2). The so prepared substrates were incubated overnight with

the purified structures of DNA-origami with AuNRs for their immobilization through DNA hybridization of the Poly-A on the surface and the free Poly-T on the AuNRs.

ASSOCIATED CONTENT

Supporting Information. Materials; synthesis of AuNRs; DNA origami design; simulated scattering spectra; additional examples of unidirectional antennas; simulations of F/B ratio for various NR sizes; effect of dipole orientation on F/B ratio of UUA.

AUTHOR INFORMATION

Corresponding Author

*Corresponding author. E-mail: fernando.stefani@df.uba.ar (F.D.S.), mauricio.pilopais@unifr.ch (M.P.P.), guillermo.acuna@unifr.ch (G.P.A.).

Author Contributions

F.D.S and G.P.A. conceived the experiments. F.D.S, M.P.P. and G.P.A. designed the experiments. M.P.P. and F.Z. designed and fabricated the optical antennas. F.Z. and A.I.F.D. performed the

numerical simulations. L.M.L.-M. and X.Z. provided gold nanorods for preliminary tests. M.S.P. modified the fluorescence microscope to enable back focal plane imaging. M.S.P. and F.Z. performed the measurements and analyzed the results. G.P.A. supervised the project. F.D.S. and G.P.A. wrote the manuscript with input from all the authors. All authors have given approval to the final version of the manuscript. ‡These authors contributed equally.

Funding Sources

This work was financially supported by European Union's Horizon 2020 research and innovation program (grant agreement No 861950, prUUAoject POSEIDON), MCIN/AEI /10.13039/501100011033 through Maria de Maeztu Unit of Excellence (MDM-2017-0720), Juan de la Cierva Fellowship (FJC2018-036104-I), Max Planck Society and the Alexander von Humboldt Foundation, Consejo Nacional de Investigaciones Científicas y Técnicas (CONICET) and Agencia Nacional de Promoción Científica y Tecnológica (ANPCYT) (PICT-2017-0870, and PICT-2014-3729), Spanish MCIN/AEI/10.13039/50110001033, "ERDF A way of making Europe" (grant No. RTI2018-099737-B-I00), 2020 CAM Synergy (Project Y2020/TCS-6545 NanoQuCo-CM), Swiss National Science Foundation (200021_184687) and National Center of Competence in Research Bio-Inspired Materials NCCR (51NF40_182881).

ACKNOWLEDGMENT

We thank Dr. Mathias Lakatos for fruitful discussions.

REFERENCES

(1) Koenderink, A. F. Single-Photon Nanoantennas. *ACS Photonics* **2017**, 4 (4), 710–722.

(2) Bharadwaj, P.; Deutsch, B.; Novotny, L. Optical Antennas. *Adv. Opt. Photonics* **2009**, 1, 438–483.

(3) Novotny, L.; Hecht, B. Principles of Nano-Optics; *Cambridge University Press*, **2006**.

(4) Kinkhabwala, A.; Yu, Z.; Fan, S.; Avlasevich, Y.; Müllen, K.; Moerner, W. E. Large Single-Molecule Fluorescence Enhancements Produced by a Bowtie Nanoantenna. *Nat. Photonics* **2009**, 3 (11), 654–657.

(5) Fabrizio, E. Di; Schlücker, S.; Wenger, J.; Regmi, R.; Rigneault, H.; Calafiore, G.; West, M.; Cabrini, S.; Fleischer, M.; van Hulst, N. F.; et al. Roadmap on Biosensing and Photonics with Advanced Nano-Optical Methods. *J. Opt.* **2016**, 18, 063003.

(6) Novotny, L.; van Hulst, N. Antennas for Light. *Nat. Photonics* **2011**, 5, 83–90.

(7) Koski, J. V.; Landig, A. J.; Russ, M.; Abadillo-Uriel, J. C.; Scarlino, P.; Kratochwil, B.; Reichl, C.; Wegscheider, W.; Burkard, G.; Friesen, M.; et al. Strong Photon Coupling to the Quadrupole Moment of an Electron in a Solid-State Qubit. *Nat. Phys.* **2020**, 16 (6), 642–646.

(8) Alù, A.; Engheta, N. Wireless at the Nanoscale: Optical Interconnects Using Matched Nanoantennas. *Phys. Rev. Lett.* **2010**, 104 (21), 1–4.

(9) Benson, O. Assembly of Hybrid Photonic Architectures from Nanophotonic Constituents. *Nature* **2011**, 480 (7376), 193–199.

(10) Curto, A. G.; Volpe, G.; Taminiau, T. H.; Kreuzer, M. P.; Quidant, R.; van Hulst, N. F. Unidirectional Emission of a Quantum Dot Coupled to a Nanoantenna. *Science* **2010**, 329, 930–933.

(11) Taminiau, T. H.; Stefani, F. D.; Hulst, N. F. Van. Enhanced Directional Excitation and Emission of Single Emitters by a Nano-Optical Yagi-Uda Antenna. *Opt. Express* **2008**, 16 (14), 16858–16866.

(12) Maksymov, I. S.; Staude, I.; Miroshnichenko, A. E.; Kivshar, Y. S. Optical Yagi-Uda Nanoantennas. *Nanophotonics* **2012**, 1 (1), 65–81.

(13) Li, N.; Lai, Y.; Lam, S. H.; Bai, H.; Shao, L.; Wang, J. Directional Control of Light with Nanoantennas. *Adv. Opt. Mater.* **2021**, 9 (1), 1–32.

(14) Krasnok, A. E.; Miroshnichenko, A. E.; Belov, P. A.; Kivshar, Y. S. All-Dielectric Optical Nanoantennas. *Opt. Express* **2012**, 20 (18), 20599–20604.

(15) Yao, K.; Liu, Y. Controlling Electric and Magnetic Resonances for Ultracompact Nanoantennas with Tunable Directionality. *ACS Photonics* **2016**, 3 (6), 953–963.

(16) Pakizeh, T.; Käll, M.; Ka, M.; Käll, M. Unidirectional Ultracompact Optical Nanoantennas. *Nano Lett.* 2009, 9 (6), 2343–2349.

(17) Rothemund, P. W. K. Folding DNA to Create Nanoscale Shapes and Patterns. *Nature* **2006**, 440, 297–302.

(18) Pilo-Pais, M.; Acuna, G. P.; Tinnefeld, P.; Liedl, T. Sculpting Light by Arranging Optical Components with DNA Nanostructures. *MRS Bull.* **2017**, 42 (12), 936–942.

(19) Kuzyk, A.; Jungmann, R.; Acuna, G. P.; Liu, N. DNA Origami Route for Nanophotonics. *ACS Photonics* **2018**, 5 (4), 1151–1163.

(20) Prodan, E.; Radloff, C.; Halas, N. J.; Nordlander, P. A Hybridization Model for the Plasmon Response of Complex Nanostructures. *Science* **2003**, 302 (5644), 419–422.

(21) Lieb, M. A.; Zavislan, J. M.; Novotny, L. Single-Molecule Orientations Determined by Direct Emission Pattern Imaging. *J. Opt. Soc. Am. B* **2004**, 21 (6), 1210.

(22) Cai, Y.-Y.; Liu, J. G.; Tauzin, L. J.; Huang, D.; Sung, E.; Zhang, H.; Joplin, A.; Chang, W.-S.; Nordlander, P.; Link, S. Photoluminescence of Gold Nanorods: Purcell Effect Enhanced Emission from Hot Carriers. *ACS Nano* **2018**, 12, 55.

(23) Kullock, R.; Ochs, M.; Grimm, P.; Emmerling, M.; Hecht, B. Electrically-Driven Yagi-Uda Antennas for Light. *Nat. Commun.* **2020**, 11 (115), 1–7.

(24) Prakash Gurunarayanan, S.; Verellen, N.; Zharinov, V. S.; James Shirley, F.; Moshchalkov, V. V; Heyns, M.; Van de Vondel, J.; Radu, I. P.; Van Dorpe, P. Electrically Driven Unidirectional Optical Nanoantennas. *Nano Lett.* **2017**, 17, 7433–7439.

(25) Zhu, F.; Sanz-Paz, M.; Fernandez-Dominguez, A.; Pilo-Pais, M.; Acuna, G. P. Optical Ultracompact Directional Antenna Based on a Dimer Nanorod Structure. *arXiv* **2022,** 2204.02347, 1-33.

(26) Gopinath, A.; Miyazono, E.; Faraon, A.; Rothemund, P. W. K. Engineering and Mapping Nanocavity Emission via Precision Placement of DNA Origami. *Nature* **2016**, 535 (7612), 401–405.

(27) Gopinath, A.; Rothemund, P. W. K. Optimized Assembly and Covalent Coupling of Single-Molecule DNA Origami Nanoarrays. *ACS Nano* **2014**, 8 (12), 12030–12040.

(28) Vaskin, A.; Kolkowski, R.; Koenderink, A. F.; Staude, I. Light-Emitting Metasurfaces. *Nanophotonics* **2019**, 8 (7), 1151–1198.

(29) Xu, A.; Harb, J. N.; Kostiainen, M. A.; Hughes, W. L.; Woolley, A. T.; Liu, H.; Gopinath, A. DNA Origami: The Bridge from Bottom to Top. *MRS Bull.* **2017**, 42 (12), 943–950.

(30) Chen, Y.; Sun, W.; Yang, C.; Zhu, Z. Scaling Up DNA Self-Assembly. *ACS Appl. Bio Mater.* **2020**, 3 (5), 2805–2815.

(31) Kurvits, J. A.; Jiang, M.; Zia, R. Comparative Analysis of Imaging Configurations and Objectives for Fourier Microscopy. *J. Opt. Soc. Am. A* **2015**, 32 (11), 2082.

(32) Douglas, S. M.; Marblestone, A. H.; Teerapittayanon, S.; Vazquez, A.; Church, G. M.; Shih, W. M. Rapid Prototyping of 3D DNA-Origami Shapes with CaDNAno. *Nucleic Acids Res.* **2009**, 37 (15), 5001–5006.

(33) Castro, C. E.; Kilchherr, F.; Kim, D.-N.; Shiao, E. L.; Wauer, T.; Wortmann, P.; Bathe, M.; Dietz, H. Quantitative Prediction of 3D Solution Shape and Flexibility of Nucleic Acid Nanostructures. Nucleic Acids Res. **2012**, 40 (7), 2862–2868.

(34) Poppleton, E.; Mallya, A.; Dey, S.; Joseph, J.; Sulc, P. Nanobase.Org: A Repository for DNA and RNA Nanostructures. Nucleic Acids Res. **2022**, 50 (database issue), D246–D252.

(35) González-Rubio, G.; Kumar, V.; Llombart, P.; Díaz-Núñez, P.; Bladt, E.; Altantzis, T.; Bals, S.; Peña-Rodríguez, O.; Noya, E. G.; MacDowell, L. G.; et al. Disconnecting Symmetry Breaking from Seeded Growth for the Reproducible Synthesis of High Quality Gold Nanorods. ACS Nano **2019**, 13 (4), 4424–4435.

(36) Liu, B.; Liu, J. Freezing Directed Construction of Bio/Nano Interfaces: Reagentless Conjugation, Denser Spherical Nucleic Acids, and Better Nanoflares. J. Am. Chem. Soc. **2017**, 139, 9471–9474.

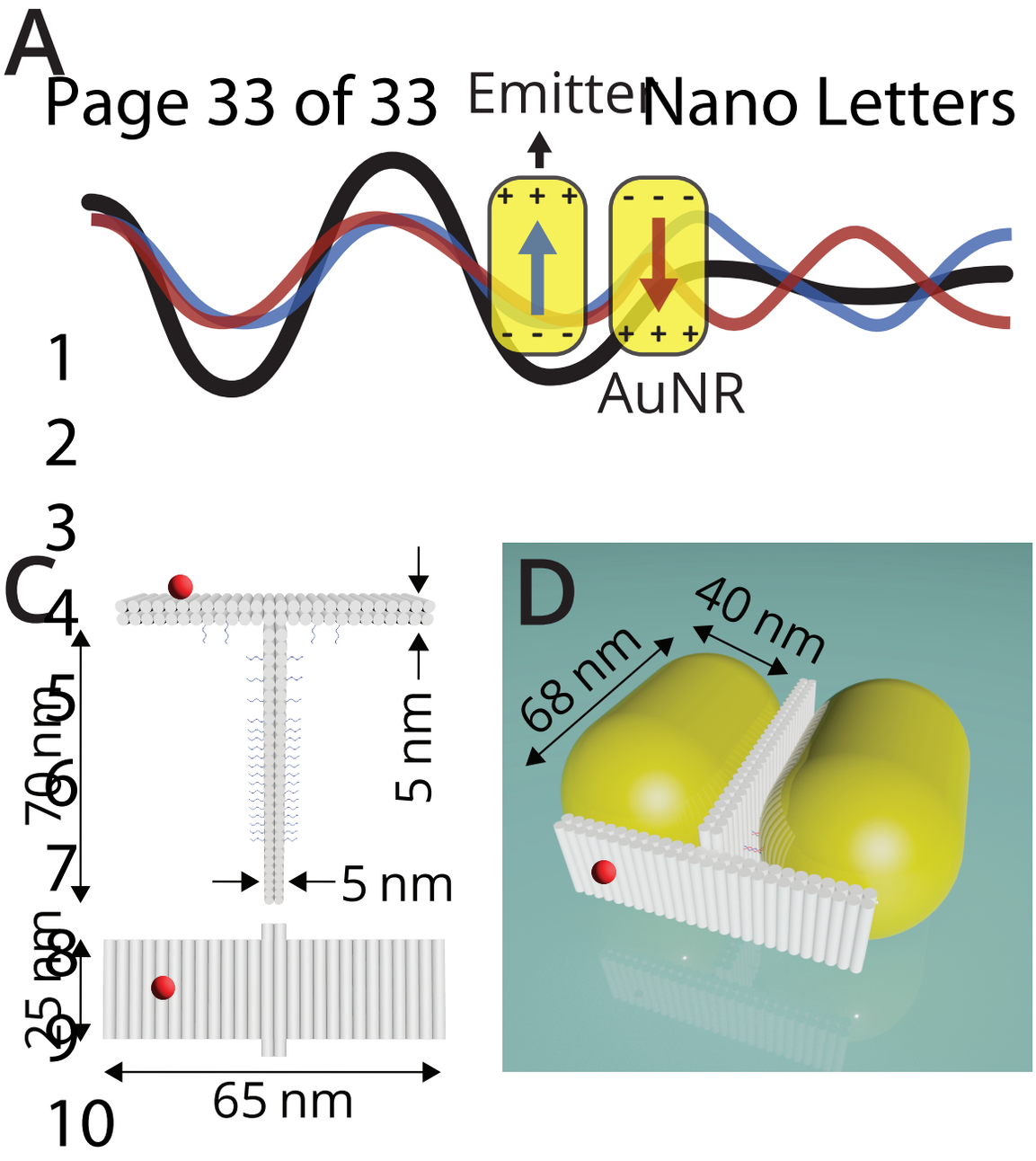
A
Emitter
AuNR
B
C
5 nm
70 nm
5 nm
25 nm
65 nm
D
68 nm
40 nm
E
F
620 nm
700 nm
Directivity
15
12
9
6
3
0
550
600
650
700
Wavelength (nm)
Emission ATTO 594
ACS Paragon Plus Environment